Available online at www.sciencedirect.com
SCIENCE DIRECT®
Journal of Non-Crystalline Solids 316 (2003) 82–95
JOURNAL OF NON-CRYSTALLINE SOLIDS
www.elsevier.com/locate/jnoncrysol

Section 4. Bulk metallic glasses

Modeling and measurement of residual stresses in a bulk metallic glass plate

C. Can Aydiner [a], Ersan Üstündag [a,*], Michael B. Prime [b], Atakan Peker [c]

[a] *Keck Lab., Department of Materials Science, California Institute of Technology, 1200 E. California Boulevard, M/C 138-78, Pasadena, CA 91125, USA*
[b] *Engineering Sciences and Applications Division, Los Alamos National Laboratory, Los Alamos, NM 87545, USA*
[c] *Liquidmetal Technologies, Lake Forest, CA 92630, USA*

Abstract

The recent advent of multi-component alloys with exceptional glass forming ability has allowed the processing of large metallic specimens with amorphous structure. The possibility of formation of *thermal tempering* stresses during the processing of these bulk metallic glass (BMG) specimens was investigated using two models: (i) instant freezing model, and (ii) viscoelastic model. The first one assumed a sudden transition between liquid and elastic solid at the glass transition temperature. The second model considered the equilibrium viscosity of BMG. Both models yielded similar results although from vastly different approaches. It was shown that convective cooling of $Zr_{41.2}Ti_{13.8}Cu_{12.5}Ni_{10}Be_{22.5}$ plates with high heat transfer coefficients could potentially generate significant compressive stresses on the surfaces balanced with mid-plane tension. The crack compliance (slitting) method was then employed to measure the stress profiles in a BMG plate that was cast in a copper mold. These profiles were roughly parabolic suggesting that thermal tempering was indeed the dominant residual stress generation mechanism. However, the magnitude of the measured stresses (with peak values of only about 1.5% of the yield strength) was significantly lower than the modeling predictions. Possible reasons for this discrepancy are described in relation to the actual casting process and material properties. The extremely low residual stresses measured in these BMG specimens, combined with their high strength and toughness, serve to further increase the advantages of BMGs over their crystalline metal counterparts.

PACS: 61.43.Dq; 81.70.Bt; 83.60.Bc; 62.20.−x

1. Introduction

Multi-component metallic alloys with superb glass formation ability have recently been developed allowing, for the first time, the processing of large specimens with amorphous structure. Referred to as bulk metallic glasses (BMGs), these materials have been shown to have impressive properties such as very high elastic strain limit (2%) and yield strength (~2 GPa), good fracture toughness (up to 55 MPa $m^{1/2}$), excellent corrosion resistance, etc. An important question that arises with bulk production is the nature and magnitude

* Corresponding author. Tel.: +1-626 395 2329; fax: +1-626 395 3933.
E-mail address: ersan@caltech.edu (E. Üstündag).

0022-3093/03/$ - see front matter
PII: S0022-3093(02)01940-3

of processing-induced residual stresses. The BMG processing typically involves casting an alloy into a mold followed by severe quenching. This procedure can lead to large thermal gradients due to the low thermal conductivity of BMG. In addition, during glass transition the alloy exhibits large changes in its viscosity within a small temperature range. All of these parameters can lead to '*thermal tempering*' which generates compressive surface residual stresses balanced with mid-plane tension.

A similar phenomenon was observed previously in silicate glasses [1]. Thermal tempering in these glasses was mostly studied for a certain initial boundary value problem: an infinite plate at a uniform initial temperature convectively cooled from both sides. The resulting stress profile was roughly parabolic where compression on the surface(s) was balanced by tension in the interior. First theories made use of the *instant freezing assumption* (see, e.g. [2]) that presumed the material behaves as a non-viscous fluid above its glass transition temperature and as a linear elastic solid below it. This simplistic approach required only the glass transition temperature as the rheological input and ignored the details of the glass transition range and its cooling rate dependence as well as any stress relaxation below that range. The theory eventually evolved with the necessary material functions (e.g., relaxation and structural moduli) [3] such that any geometry could be handled with finite element modeling [4,5].

Unfortunately, most viscoelastic properties of BMGs, especially the ones needed for advanced modeling of thermal tempering, have not yet been investigated systematically. For this reason, the instant freezing assumption was invoked first in the present study to obtain estimates of the residual stresses generated by this phenomenon. Next, the only available viscoelastic data on the BMG alloy used here, its equilibrium viscosity as a function of temperature, were employed to develop the first viscoelastic model of thermal tempering in BMGs. The model predictions were then compared to residual stress data collected from a cast BMG plate using the crack compliance method. To the authors' knowledge, this is the first extensive theoretical/experimental investigation of thermal tempering in BMGs.

2. Modeling of thermal tempering

2.1. Instant freezing model

Thermal tempering is a result of a process which involves heating glass above its *glass transition temperature* (T_g) and then rapidly cooling it. During cooling, the surfaces of a glass plate solidify and contract first, leading to tension on the surface and compression in the mid-plane. The same would occur in an elastic solid. However, in this phase of quenching a glass, the core is still of low viscosity and the mid-plane compressive stresses are simultaneously relaxed by viscous flow. Therefore, stresses developed before the entire cross-section solidifies are lower than those in an otherwise identical but elastic material with the same temperature distribution. However, when the mid-plane finally solidifies, the viscous effects cease and the material becomes practically an elastic glass plate, imposed with the temperature profile at that instant. All further changes in stresses are determined by changes in the temperature profile only. As the temperature gradients decay to a constant value at room temperature, stresses in the opposite sense are produced: tension in the mid-plane and compression on the surface. For an *always* elastic solid these would be equal and opposite to those produced in the first phase when temperature gradients grew. In a glass, which involves stress relaxation at the beginning, the two types of stresses are not equal. In other words, the stresses produced during the decay of temperature gradients have an excess over the ones produced initially. This leads to residual tension in the mid-plane and compression on the surface.

The resulting residual stress profile as a function of distance from the center of the plate is given by the instant freezing model as follows [6]:

$$\sigma(Z) = \frac{\alpha E(T_g - T_a)}{1-\nu}\left(1 - \frac{\sin\delta}{\delta} - \int_0^{Z/L} \frac{(\sin\delta - \sin\delta\zeta)\sin\delta\zeta}{(1-\zeta)\cos^2\delta\zeta}\,\mathrm{d}\zeta\right), \qquad (1)$$

where α is the coefficient of linear thermal expansion, E is the Young's modulus, ν is the Poisson's ratio, T_g is the glass transition temperature, T_a is

the ambient temperature and δ is a measure of the cooling rate. More explicitly δ is given as the first root of $\delta \tan \delta = Bi$ where $Bi = hL/k$ is the Biot number with h, L, k denoting heat transfer coefficient, half-thickness of the plate and thermal conductivity, respectively. Fig. 1 shows the in-plane residual stress profile across the plate thickness. In-plane coordinates are X and Y while Z is the out-of-plane coordinate. Thermal-tempering-induced residual stresses are equibiaxial in the X–Y plane for this infinite plate problem.

Presently, the exact values of experimental heat transfer coefficients typically found in BMG processing are unavailable. To obtain a rough estimate, a recent processing method called melt infiltration casting [7] is noted. In one version of this technique, BMG alloys are cast in stainless steel tubes and then quenched in water. This means cooling is via convection by water which flows in either laminar or turbulent manner. The heat transfer coefficient for free convection of water (i.e., stagnant water) at room temperature is about 900 W/(m^2 K) [8]. When water is forced to flow laminarly, this value can easily reach 2000–3500 W/(m^2 K). If water boils (as is sometimes observed during melt infiltration processing), then values up to 35 000 W/(m^2 K) are possible. To be conservative, $h = 2000$ W/(m^2 K) was chosen. This value for h also yields the same time scale ($\sim$10 s) it takes to cool a BMG plate from melt to room temperature as described in Section 3 when the casting procedure used in this study is mentioned. The predictions of Eq. (1) for surface compression and mid-plane tension as a function of plate thickness (t) and heat transfer coefficient (h) are shown in Figs. 2 and 3, respectively. The material parameters employed in the calculation are listed in Table 1.

The instant freezing model predictions suggest significant residual stresses can be generated in BMGs due to the thermal tempering effect. Another prediction of the instant freezing model is that as the value of surface compression increases, the thickness of the surface layer it is confined to decreases since the balancing mid-plane tension saturates (see Fig. 2). This means, a progressively thinner surface layer with an increasingly high stress gradient can be formed as the degree of temper increases.

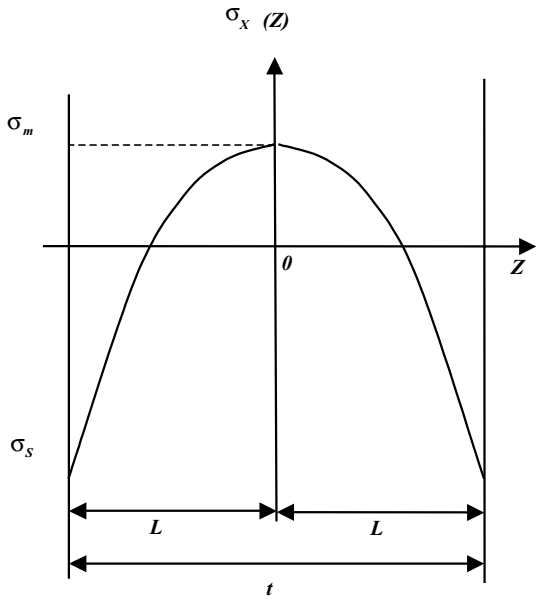

Fig. 1. A typical residual stress profile across the thickness of a large plate due to thermal tempering: surface compression (σ_s) is balanced with mid-plane tension (σ_m). The in-plane stresses are equibiaxial and function of the thickness coordinate (Z) only.

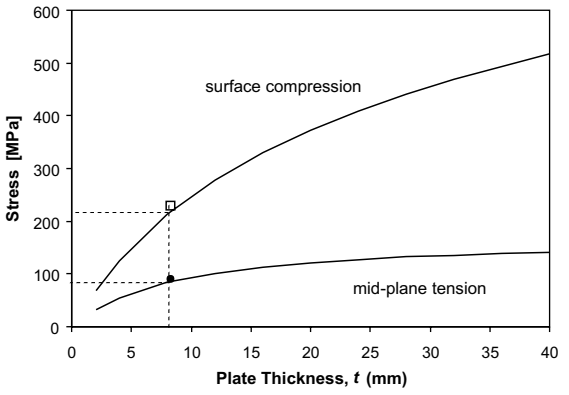

Fig. 2. Equibiaxial (absolute) stress values at the surface and mid-plane of a large $Zr_{41.2}Ti_{13.8}Cu_{12.5}Ni_{10}Be_{22.5}$ (Vit.1) plate for $h = 2000$ W/(m^2 K) as a function of plate thickness [6]. The stresses predicted by the instant freezing model for the 8.25 mm thick plate used in this study are marked with dashed lines while those predicted by the viscoelastic model are indicated by (□) and (•). The viscoelastic model calculations were performed for $\beta = 1$ in Eq. (4).

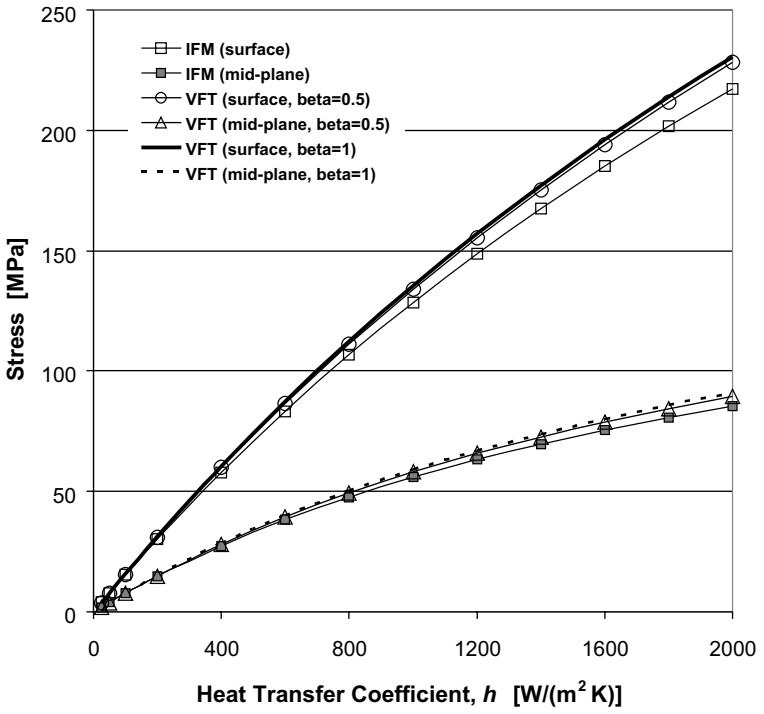

Fig. 3. Absolute values of surface and mid-plane stresses predicted by both instant freezing (IFM) and viscoelastic – VFT models of thermal tempering of an 8.25 mm thick Vit.1 plate as a function of (convection) heat transfer coefficient. The VFT data are shown for two different calculations using $\beta = 0.5$ and 1 in Eq. (4).

Table 1
Material parameters used in the modeling calculations [6]

Thermal conductivity	k	4 W/(m K)
Density	ρ	5.9 g/cm^3
Linear thermal expansion coefficient	α	10.1×10^{-6} K^{-1}
Specific heat	C_p	666 J/(kg K) at 25 °C 850 J/(kg K) at 900 °C
Glass transition temperature	T_g	352 °C
Initial (melt) temperature	T_i	900 °C
Quenching temperature	T_a	25 °C
Young's modulus	E	90 GPa
Poisson's ratio	v	0.354
Shear modulus (at room temperature)	μ_{RT}	33.2 GPa

2.2. Viscoelastic model

2.2.1. Introduction

Historically, this was the second model developed to quantify the thermal tempering of silicate glasses [9]. The viscoelastic model employed the measured rheological properties of the *equilibrium* liquid at each temperature. Hence, it replaced the awkward jump from a non-viscous fluid to a linear elastic solid in the former instant freezing models with a smooth transition. The viscoelastic model was applied to a class of materials with thermo-rheological simplicity. For such a material, the creep function, relaxation modulus and any other

characteristic viscoelastic function plotted vs. the logarithm of time exhibit only a simple shift when the temperature is changed to another constant value. Equilibrium liquids of silicate glasses (called stabilized glass) were shown to be thermorheologically simple prior to the analysis in [9].

For the tempering problem, the appropriate viscoelastic function is the shear relaxation modulus and at a certain temperature T, it will be denoted by $G_T(t)$. Bulk relaxation is typically much more sluggish than shear relaxation and Lee et al. made the reasonable assumption of elastic bulk response. Hence in this problem, the viscoelastic behavior of the material over the entire temperature range is obtained using two material functions only. The first is the shear relaxation modulus measured at a reference temperature, T_R, denoted by $G_{TR}(t)$ and the second is the 'shift function', $a(T)$, which bears the temperature dependence. It shifts the reference function $G_{TR}(t)$ in logarithm of time to obtain $G_T(t)$, namely, the relaxation modulus at the temperature of interest.

2.2.2. Viscoelastic model for bulk metallic glass

The authors are not aware of any definitive data on isothermal measurements of shear relaxation moduli for $Zr_{41.2}Ti_{13.8}Cu_{12.5}Ni_{10}Be_{22.5}$ (Vit.1™) at various temperatures. Therefore, this model considers the equilibrium viscosity of this alloy which has been thoroughly studied with creep tests around the glass transition and rotating cup experiments about the melting point [10–12]. The viscosity data covers a range of 14 orders of magnitude and is successfully fit with the Vogel–Fulcher–Tammann (VFT) relation as follows:

$$\eta(T) = \eta_0 \exp\left(\frac{D^* T_0}{T - T_0}\right), \tag{2}$$

where D^* is called the fragility parameter and T_0 is the VFT kinetic freezing temperature. The value of η_0 is 4×10^{-5} Pa s and the best fits to experimental viscosity data yield $D^* = 18.5$ and $T_0 = 412.5$ K [10].

Since the steady-flow viscosities were measured with creep tests in the temperature range of interest, the following relation between viscosity and relaxation modulus at temperature T holds [13]:

$$\eta(T) = \int_0^\infty G_T(t)\,\mathrm{d}t. \tag{3}$$

The determination of the relaxation modulus from the scalar viscosity data is not possible. Therefore, the analysis was pursued as a parametric study for the relaxation time spectrum. In other words, a set of relaxation moduli with varying spectra were considered for residual stress calculations such that they satisfied Eq. (3). To conveniently cover a broad range of relaxation spectra, the Kohlrausch–Williams–Watts (KWW) form was assumed for the relaxation modulus:

$$G_T(t) = \mu(T) \exp[-(t/\tau(T))^\beta], \tag{4}$$

where β is the stretching exponent and $\mu(T)$ is the instantaneous shear modulus at T. $\beta = 1$ corresponds to Debye relaxation and the spectrum broadens as β decreases. $\tau(T)$ is calculated by substituting Eq. (4) in Eq. (3) as follows:

$$\tau(T) = \frac{\eta(T)}{\mu(T)} \frac{1}{\Gamma(1 + 1/\beta)}. \tag{5}$$

Calculations were carried out for β values that systematically varied in increments of 0.05 in the $0.5 \leqslant \beta \leqslant 1$ range. First, the temperature dependence of the shear modulus was neglected and its room temperature value ($\mu_{RT} = 33.2$ GPa) was used. This was one of the assumptions made by Narayanaswamy [3] in his analysis of silicate glass tempering after noting Kurkjian's data [14] that showed ≈15% decrease in the shear modulus of glass as its temperature approached the glass transition region. Recently, a similar decrease (10–20%) in the elastic modulus of some metallic glasses has been measured as the temperature reached T_g [15]. To investigate the sensitivity of the residual stresses to such changes in the shear modulus, a second set of computations was made by assuming a linear variation of the shear modulus from $\mu_{RT} = 33.2$ GPa at room temperature to $0.85\mu_{RT}$ (= 28.2 GPa) at T_g. These calculations were performed for a heat transfer coefficient of $h = 2000$ W/(m^2 K). The results showed that the effect of shear modulus variation with temperature was negligible as far as the final residual stress values were concerned (the change was less than

0.25%). Therefore, this effect is excluded from the discussion that follows.

The viscoelastic model calculations were performed using the finite element method and the details are described in the next section. The comparison of results obtained from both the instant freezing and viscoelastic models is exhibited in Fig. 3. It is seen that the predicted residual stresses are rather insensitive to the value of the Kohlrausch factor, β, for the range of β values considered ($0.5 \leqslant \beta \leqslant 1$). The variation in mid-plane tension and surface compression with β in this range is under 1.6% and 1.3%, respectively (the calculated stresses increase when β changes from 0.5 to 1).

Note that any possible temperature dependence of the Kohlrausch factor β was not considered in the above parametric study. This was done to preserve the thermorheological simplicity assumption. Allowing for the temperature variation of β invalidates thermorheological simplicity and excessively complicates the calculations impeding the use of the current numerical method. Furthermore, the extremely weak dependence of the solution on β justifies this negligence of its variation with temperature.

Finally, all the arguments presented above assume the thermal stability of the BMG alloy throughout the quenching process, and phenomena such as phase separation [10,11] were not considered. In addition, the non-linear viscous response (e.g., shear thinning) of the material [16] due to high shear rates was also ignored.

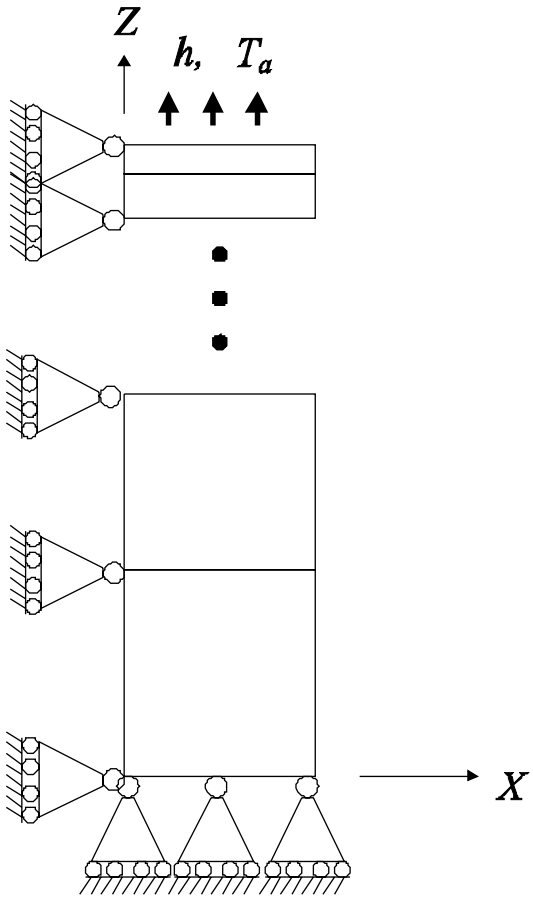

Fig. 4. Schematic of the finite element model used in viscoelastic model calculations. An infinite plate is represented via symmetric elements (in X and Y) while the plate half-thickness extends along Z. The elements (or nodes) on the right-hand side are required to move uniformly along the X-direction.

2.2.3. Implementation of the viscoelastic model for bulk metallic glass

The calculations for the viscoelastic model were conducted using the ABAQUS finite element software. A one-dimensional model was built (see Fig. 4) to represent an infinite plate. The elements were arranged along the plate thickness direction (Z) with symmetry imposed on both perpendicular directions (X and Y). To implement the compatibility condition for the infinite plate, first, the right side nodes were constrained to deform as a line. Second, unlike regular plane strain elements where the displacements in the Y-direction would merely be set to zero, *generalized* plane strain elements were used that allowed uniform deformation in the out-of-plane direction Y. The lengths of the elements along the Z-direction were biased such that the mesh became finer towards the surface where there are higher temperature gradients. The cooling of the plate was carried out via convection heat transfer applied on the top surface. Thermorheological simplicity in ABAQUS was defined for the relaxation function, namely, relaxation modulus normalized by its instantaneous value was given by $\exp(-t/\tau)^{\beta}$ in the KWW formalism. This way, the use of temperature-dependent shear modulus $\mu(T)$, which invalidates thermorheological simplicity for

relaxation modulus but not relaxation function, did not pose any additional difficulties. The relaxation function was calculated and input to the program at a reference temperature T_R and the shift function given below was implemented with a user-defined subroutine:

$$a(T) = \frac{\tau(T)}{\tau(T_R)} = \frac{\mu(T_R)}{\mu(T)} \exp\left[D^* T_0 \left(\frac{1}{T_R - T_0} - \frac{1}{T - T_0}\right)\right]. \quad (6)$$

The material data shown in Table 1 were applied for the Vit.1 plate of interest (thickness = 8.25 mm) using this model to obtain the following values for surface compression and mid-plane tension at $h = 2000$ W/(m^2 K): $\sigma_s \approx -230$ MPa and $\sigma_m \approx +90$ MPa. These results are also shown in Fig. 2. In addition, the heat transfer coefficient (h) was varied while keeping the plate thickness fixed at 8.25 mm (Fig. 3).

3. Specimen preparation

A $Zr_{41.2}Ti_{13.8}Cu_{12.5}Ni_{10}Be_{22.5}$ (Vit.1™) plate was used in this study to measure the tempering-induced residual stresses. This plate was nominally 150 mm long, 100 mm wide and 8.25 mm thick. It was cast using a large copper mold that was initially at room temperature. Due to the proprietary nature of the process, only details relevant to this publication are discussed here. The alloy melt was fed into the copper mold at low pressure by vacuum assistance. A solid skin of Vit.1 likely formed at the cavity surfaces as the molten alloy flowed into the mold. The skin thickness was expected to be inversely proportional to the thickness of the plate, i.e., the thickness of the thermal mass fed into the mold. Filling up the mold was estimated to take 2–3 s. The feeding pressure was kept for another 10 s to allow sufficient solidification of the plate such that it could be retained in the mold cavity. The plate surfaces possibly separated from the cavity surfaces during this process due to the larger thermal contraction of the BMG above its glass transition ($\alpha_{Vit.1} = 17.7 \times 10^{-6}$ K^{-1} [17]) and the low initial average temperature of the mold. Final cooling to room temperature was achieved by quenching the mold in water. Since the coefficient of thermal expansion of copper ($\alpha_{Cu} = 16.5 \times 10^{-6}$ K^{-1} [18]) is larger than that of Vit.1 ($\alpha_{Vit.1} \cong 10 \times 10^{-6}$ K^{-1} below its glass transition [17]), the mold likely pressed on the plate during quenching.

4. Residual stress measurement using crack compliance method

Residual stresses in BMGs cannot be conveniently determined by non-destructive methods. While photoelasticity could be used in silicate glasses to measure both residual and in situ stress profiles during processing [1], the opacity of BMGs prevents the use of this method. Diffraction is similarly not applicable since BMGs are amorphous. Therefore, mechanical relaxation methods remain as the only options to obtain the stress profile within the desired spatial resolution. These methods rely on disturbing the equilibrium of a sample under residual stress by removing material in a particular way. The deformation of the sample as it reaches a new equilibrium is then monitored and this information is used to back-calculate the original residual stresses. The crack compliance method [19,20] was chosen in this study since it allows accurate determination of the complete through-thickness profile with good spatial resolution in the measurement direction.

In this method, strains are measured as a slit is incrementally cut through a specimen. Assuming that the stress relaxation from cutting the slit is elastic, the original profile of residual stress is calculated from the measured strains. Fig. 5 illustrates a crack compliance measurement and defines the terminology. A slit is introduced, and its depth a in the Z-direction is extended incrementally. The test is used to determine $\sigma_X(Z)$ through the thickness of the specimen. Two strain gauges are employed. The top strain gauge, placed very near the cut, is used for determining the stresses in the near surface region ($a/t < 0.05$). The back gauge is placed directly opposite to the cut and is used to calculate the stresses through the remaining portion of the specimen.

The original residual stresses are determined from the measured strains using the series expan-

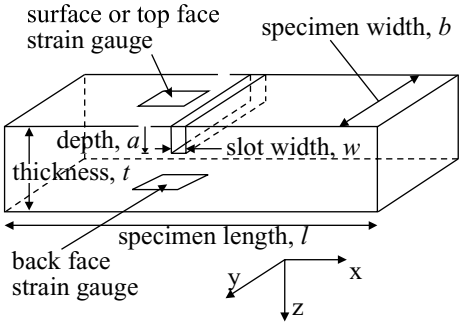

Fig. 5. Crack compliance method terminology (adapted from [19]).

sion approach [19,21], which is very tolerant of noise and errors in the experimental strain data. It is first assumed that the unknown stress variation as a function of the through-thickness coordinate can be expressed as a series expansion:

$$\sigma_x(Z) = \sum_{i=1}^{n} A_i P_i(Z) = [P]\{A\}, \tag{7}$$

where the A_i represent unknown series coefficients. For this study, Legendre polynomials expanded over the thickness of the plates were chosen for the P_i because, by excluding the 0th and 1st order polynomials, the resulting stress distribution is guaranteed to satisfy force and moment equilibrium. The strains that *would* be measured at the cut depths a_j are calculated for each term in the series. These are called the compliance functions C_{ij}. Using superposition, the strains given by the series expansion can be written as

$$\varepsilon_x(a_j) = \sum_{i=1}^{n} A_i C(a_j, P_i) = [C]\{A\}. \tag{8}$$

A least squares fit to minimize the error between the strains given by Eq. (8) and the measured strains yields the A_i (and hence the stresses by Eq. (7)) and can be written as

$$\{A\} = ([C]^{\mathrm{T}}[C])^{-1}[C]^{\mathrm{T}}\{\varepsilon_{\mathrm{measured}}\}. \tag{9}$$

In this study, the compliance functions for the top strain gauge were calculated using a numerical, body-force method solution for a slot in a semi-infinite solid [22] with some improvements made to the numerical solution [23]. The compliance functions for the back strain gauge were calculated by two-dimensional finite element calculations of a crack in a plate. Uncertainties in the final stress prediction were based on standard error propagation formulas applied to the above equations using the difference between the measured and calculated (Eq. (8)) strains as the measurement uncertainty [24]. Using too low an order, n in Eq. (7), of an expansion results in not fitting the measured strains well and, therefore, leads to large uncertainties in the stresses. Inversely, using too high of an order results in a more singular matrix inverse, Eq. (9), and also large uncertainties in the stresses. Thus, an optimal fit order was chosen to minimize uncertainty.

The cuts were made using wire electric discharge machining (EDM), which is preferred over mechanical cutting. The machine was set to 'skim cut' settings to minimize stresses induced during cutting [25]. It must be mentioned that the dimensional accuracy of the samples was not perfect since they were extracted from a cast plate. The thickness of the sample in the cut plane varied within 0.1 mm for most samples. The cut depth and thickness values were based on accurate measurements performed with an optical microscope from both sides of the sample.

Fig. 6, which is roughly to scale, shows the original locations of samples extracted from the plate. The seven samples tested for through-thickness stress profiles in the Y-direction were named $\mathrm{Y1},\ldots,\mathrm{Y7}$, and similarly the four samples tested in the X-direction were called $\mathrm{X1},\ldots,\mathrm{X4}$. One face of the plate was selected as the top and was kept as such for all samples except Y7, X2 and X4 that were intentionally slit from the other side to check the symmetry of the stress profile. Sample A1 was annealed at 290 °C for 2 h to relieve the residual stresses. This temperature is high enough to allow rapid stress relaxation [26] without significantly changing the structure of Vit.1. The amorphous structure of A1 after heat treatment was confirmed with X-ray diffraction. The samples were nominally 25.4 mm long by 12.7 mm wide. The sample length, l, was large enough ($l/t \sim 3$) to substantially preserve the original residual stresses in the measurement direction on the cut plane [27]. Also the width dimension, b, was large enough to

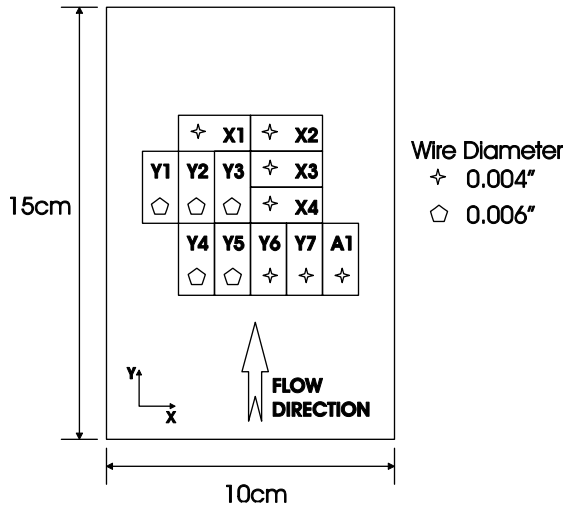

Fig. 6. Locations of samples in the plate before cutting. Plate dimensions are: 150 mm by 100 mm by 8.25 mm. Wire diameters used in cutting each sample are indicated in inches. The flow direction of the molten BMG during casting is also shown. The samples are 12.7 mm by 25.4 mm. The ones designated by X were used to determine in-plane stresses along the X-direction (σ_X), while those named Y1, etc. were used to measure σ_Y.

conform to the plane strain assumption used in the calculations [27]. While the earlier tests employed a 0.006 in. (0.150 mm) diameter wire, the later ones used a 0.004 in. (0.100 mm) diameter wire (see Fig. 6 about a distribution of samples for each). The slot was cut in 0.254 mm increments. This value was reduced to 0.127 mm during the first few steps to obtain a higher resolution near the top surface.

5. Experimental results

The top gauge did not yield reliable data in some early tests. This was attributed to the poor attachment and coating of the gauge which prevented its waterproof installation. The EDM machine used in these tests employed a water jet to keep the wire-workpiece region engulfed in a dielectric fluid. Fortunately, most of the data come from the back gauge (from 10% to 90% of the thickness of the sample) and a top gauge is not strictly necessary. Therefore, almost the complete stress profile can be obtained using only back gauge data. The disadvantages in this case are that the precision in the near-surface stresses is low and the stabilizing effect of the top gauge on the solution is lost. Nevertheless, the uncertainty analysis correctly accounts for such issues. In this study, it was seen that the accuracy of the mid-plane stresses was still quite good and the trend of the stress profile was adequately resolved. On the other hand, the tests for samples X1, X2, X4, Y7 and A1 were successful in yielding data from both gauges and the results obtained from the first four of these samples are similar to those obtained from all other as-cast specimens.

The back gauge strain profiles from all specimens are shown in Fig. 7. It is worth noting that the profiles for all samples, tested both in X- and Y-directions (except the stress-relieved A1), exhibited remarkable similarity in shape and magnitude even though a few of the tests, e.g., that of Y6 and X4, yielded somewhat lower quality data. This shows, first, that the stress profile has weak X–Y coordinate (spatial) dependence and it also suggests that the stress state is approximately equibiaxial. Note that if samples with stress profiles that are merely multiples of each other are considered, back gauge strain vs. normalized depth data will scale linearly with the amplitude of these stress profiles. On the other hand, top gauge data are not directly comparable for their values will also depend on the gauge-to-slot distance.

Typical stress profiles obtained from the back gauge data of specimens Y2, Y3, Y4 are shown in Fig. 8(a). These tests yielded particularly clean data and reduction of the stress profile was straightforward. In Fig. 8(b), the test of Y7 is compared with that of the annealed sample, A1. Since the top gauge worked in both tests, the stresses on the top surface are also exhibited. The error bars in Fig. 8 are seen to be much smaller than the observed stress profile. More significantly, the apparent stress variation in the annealed specimen (A1) is within 5 MPa indicating the stress resolution of the crack compliance method.

Note that only stress values that are significant are plotted. This involves excluding a number of points near the top surface where the back gauge response is too weak (for the tests where the top gauge did not function properly) and a few points close the full thickness of the sample where the

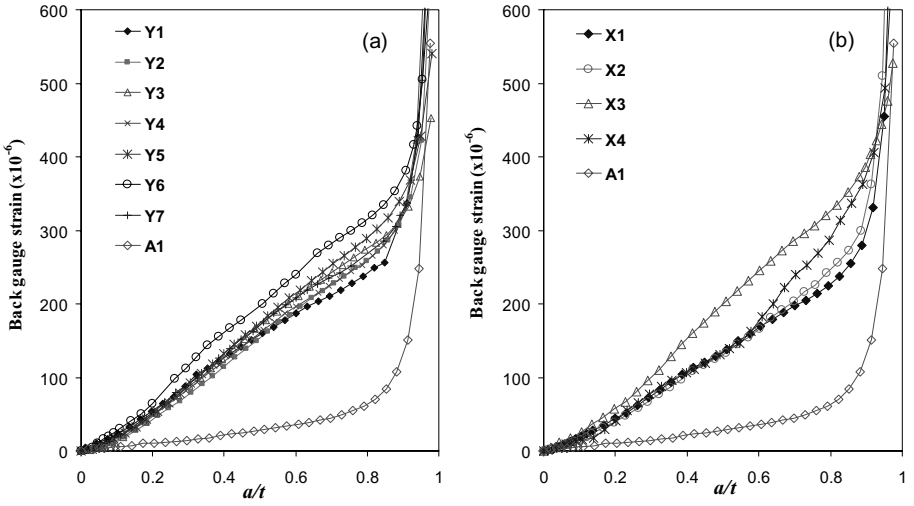

Fig. 7. Back strain vs. normalized depth data for samples (a) in the Y-direction, and (b) in the X-direction, in comparison to the annealed sample A1. See Fig. 6 for original specimen locations on the plate.

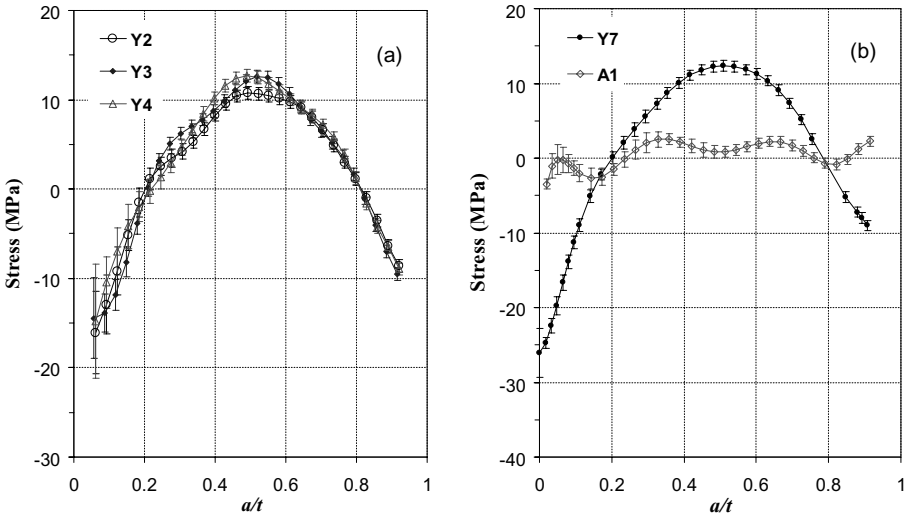

Fig. 8. (a) Calculated stress profile vs. normalized depth reduced from the back gauge strain data only. (b) The stress profile obtained from both top and back gauges.

strains no longer give a good estimate of the residual stress. As the remaining ligament (t–a in Fig. 5) becomes small, several factors (e.g., the weight of the specimen and tension in the lead wires) increasingly contribute to the strain measured by the back strain gauge by causing bending and torsion of the remaining ligament. In small samples such as these, additional stiffness from the gauge coating can also affect the strain readings as the remaining ligament becomes small. The net effect of the remaining ligament becoming small is that the experimentally measured strains become

singular as the cut approaches the back face, see Fig. 7, whereas without these effects the strain would approach a finite value (surface stress divided by plane strain elastic modulus) as the cut neared the opposite surface. In these specimens, the singular effects became significant after about $a/t = 0.92$; therefore, stresses are not reported beyond that depth.

As seen in Fig. 7, especially samples Y6 and X4 do not follow the generally observed smooth profile. Their data show awkward changes in slope and some especially bad data points were deleted. Later it was realized that the reason was variations in the flow of the dielectric fluid and formation of bubbles on the gauge surfaces as the EDM wire moved into the sample. This happened only for a few samples because the wax coating on the gauges of these samples had apparently a rougher surface that caused complicated flow patterns. Some samples such as the ones in Fig. 8(a) were usually very stable. Caution should be exercised when inverting the stresses from problematic strain data as fitting the noise will result in a wavy profile instead of the simple 'compression on the surface, tension in the middle' distribution.

The next source of error that was valid for all samples is called the 'EDM effect'. During EDM cutting, a thin material layer (with a new stress state) can be recast on the cut surfaces. This especially affects the top gauge data while the back gauge is relatively insensitive. The data from the test on the annealed specimen – very small strains measured by the back gauge and inconsistently large values from the top gauge – confirmed the likelihood of an EDM effect. The consistency of bottom gauge results for tests made with both 0.004 and 0.006 in. diameter wires also corroborates that the back gauge data were unaffected. An EDM correction detailed in [25] was performed to the top gauge strains in order to obtain the stress profiles shown in Fig. 8(b). The profile of strain as a function of cut depth that is caused by an EDM effect is quite different from the profile caused by residual stresses. It can be estimated analytically and separated out from the measured strains.

Several factors combined to make the EDM effect an issue in these tests, whereas it is usually insignificant [25]. The major factor is that the residual stresses are so low in the tested specimens. The strains caused by the EDM effect are generally a fixed small value, independent of the residual stress magnitudes, when cutting is performed gently. Thus, they generally comprise an insignificant portion of the measured strains and do not have a noticeable effect on the results. When the stresses are extremely low, as in the tests reported here, the EDM strains can contribute significantly to the measured data and, therefore, affect the results. The other factor is that the EDM effect is, other parameters equal, greater for materials with higher yield stress and low thermal conductivity, both of which apply to the BMG specimens. Even so, if the residual stresses were higher, the EDM effect would have been negligible.

6. Discussion

Figs. 2 and 3 exhibit the predictions of both the instant freezing and viscoelastic models. Despite vastly different approaches and the use of independent data in each, their similarity is remarkable. For instance, the shapes of the stress vs. heat transfer coefficient plots in Fig. 3 are almost identical. The model predictions, however, are significantly different than the experimental results. It was initially assumed that convective cooling with a heat transfer coefficient of $h = 2000$ W/(m^2 K) from traction-free surfaces throughout the production process of BMGs represented a reasonable estimate [6]. This value was chosen such that the imagined convective cooling of Vit.1 from melt to room temperature lasted a time period that roughly approximates the cooling duration of the actual casting process ($\sim$10 s). As observed in Fig. 2, the prediction of the instant freezing model for this 8.25 mm thick plate is -217 MPa surface compression and $+85$ MPa midplane tension, while the same stresses are estimated to be about -230 MPa on the surface and $+90$ MPa in the interior using the viscoelastic model. Note that especially the value of surface compression is highly dependent on h. However, the experimental results with $+10$ to $+13$ MPa midplane tension and -25 to -30 MPa surface compression are much smaller than model predictions.

This discrepancy is likely due to the two constituents that define the thermal tempering problem: specimen preparation procedure and material properties.

The casting process described above does not involve convective cooling on traction-free surfaces. Actually, it is more similar to the injection molding process used in the polymer industry [28,29]. For polymers, the residual stresses are classified as flow-induced stresses and residual thermal stresses. Flow-induced stresses are the stresses generated during the filling stage of the mold whereas the residual thermal stresses are due to the differential cooling of the material, which is the only case for the thermal tempering problem. It is noted in [29] that the flow stresses are an order of magnitude lower than the thermal stresses in absolute value. This is not surprising since the existence of flow at considerable rates indicates that most of the material still has very short shear stress relaxation times, and thus, is not able to accumulate residual stresses. Based on this argument, it is likely that the residual stresses that form in the BMG plate are also mostly thermal residual stresses. The fact that the measured stress profiles have no significant spatial and directional dependence within the plate gives credence to this conclusion. Furthermore, the observed 'compression–tension–compression' stress profile is typical of thermal tempering [1,6]. The thin layer of surface tension that forms in injection molding of polymers superimposed on this type of stress profile was not observed in this study.

The above arguments present the idea that although the actual casting process did not resemble the thermal tempering case considered by the models, the majority of the residual stresses were still due to thermal tempering. However, although the stress generation mechanism was the same, the thermal problem was not. In other words, the temperature profile evolution in the modeling calculation and that found in the actual sample were likely different. The convective cooling problem considered by the calculations yields an exponentially decreasing cosine profile after higher order terms decay quickly [6]. The actual quenching realized by conduction to a large copper block initially at room temperature is more complicated. An understanding of the temperature evolution is crucial for the generation of residual stresses as thermal tempering is driven by thermal gradients, or in more simple terms, the differential between the surface and mid-plane temperatures. The low magnitude of measured stresses suggests a relatively flat temperature profile about the glass transition of Vit.1 existed during the casting. There are two possible sources of such a temperature profile. First, the contact between the plate and the mold surface was likely lost some time during the process. This would result from the larger thermal contraction (especially above the glass transition) of the plate compared to the large copper mold which probably remained at relatively low temperatures. After this separation, the heat transfer from the plate to the vacuumed mold cavity would be significantly reduced. The second, and more obvious, source of a flat temperature profile in the plate is a possible increase of the temperature of the copper block. This would result in hindered heat transfer especially at low temperatures. These results point to the need for an instrumented casting experiment during which the exact temperature profile of BMG can be monitored in situ. This work is currently in progress.

Both instant freezing and viscoelastic models disregard a critical component of glass behavior: its structural relaxation from a metastable amorphous solid to a supercooled liquid in thermodynamic equilibrium [10,11]. During this process, the excess free volume trapped in the material is relaxed by short range atomic movement leading to a denser, more viscous solid. In viscoelastic theory, data for the viscoelastic behavior of the *equilibrium* material at every temperature is employed. This means, structural relaxation has already completed when equilibrium is reached. Therefore, just from viscosity point of view, the viscoelastic model employed in this study is expected to overestimate the temper stresses with respect to a more advanced structural model which can accurately consider the transient effects during structural relaxation. Unfortunately, no reliable data exist on BMGs to apply a structural model and to obtain a more realistic estimate of the tempering-induced residual stresses. Current research at Caltech

involves the generation of such data for the particular BMGs studied here.

Finally, it is worth mentioning the fact that lack of high temper stresses in BMGs is not necessarily a disadvantage. Conventional (crystalline) metals typically have residual stresses on the order of 25–50% of their yield strength [27,30]. Such stresses contribute to failure by fracture, fatigue, stress corrosion cracking, and other stress-driven processes [31]. These stresses are also a major source of expensive distortion problems caused during machining to final shape [32]. Stress relief in conventional metals, by thermal treatment or by cold working [18,33], is generally expensive and often not possible because it can significantly degrade mechanical properties. By contrast, the peak residual stresses measured in BMGs in this study only amount to about 1.5% of the yield strength. From a distortion and mechanical failure point of view, such low stresses can effectively be neglected.

7. Conclusions

This investigation of thermal-tempering-induced residual stresses in a thick BMG plate had two premises: (i) to accurately measure the residual stresses in BMG samples, and (ii) to compare the results with appropriate theory and obtain insight about the processing method and the material properties. The first was accomplished by the use of the crack compliance method, which is capable of yielding through-thickness stress profiles. The method is applicable with wire EDM cutting taking advantage of the fair electrical conductivity of BMGs. Although the measured stress magnitudes were low, the technique yielded good resolution.

Both the instant freezing and viscoelastic models employed in this study overestimated the residual stresses. This discrepancy is attributed to the lack of information about the details of processing conditions (e.g., exact value of the heat transfer coefficient on the surface) as well as the absence of an appropriate constitutive law for the BMG alloy. The viscoelastic and structural properties of BMGs have to be taken into account for a more accurate description of thermal tempering. Instrumented casting under well-defined conditions and material testing to generate viscoelastic BMG data suitable for more advanced thermal tempering models are necessary for a complete understanding of this phenomenon in BMGs.

Acknowledgement

This study was supported by the Center for Structural Amorphous Metals (Army Research Office grant no. DAAD19-01-0525) at the California Institute of Technology.

References

[1] R. Gardon, in: D.R. Uhlmann, N.J. Kreidl (Eds.), Glass Science and Technology, Elasticity and Strength in Glasses, vol. 5, Academic Press, New York, 1986, p. 146.
[2] B.D. Aggarwala, E. Saibel, Phys. Chem. Glasses 2 (1961) 137.
[3] O.S. Narayanaswamy, J. Am. Ceram. Soc. 61 (1978) 146.
[4] T.F. Soules, R.F. Busbey, S.M. Rekhson, A. Markovsky, M.A. Burke, J. Am. Ceram. Soc. 70 (1987) 90.
[5] L. Daudeville, H. Carre, J. Therm. Stresses 21 (1998) 667.
[6] C.C. Aydiner, E. Ustundag, J.C. Hanan, Metall. Mater. Trans. A 32 (2001) 2709.
[7] R.B. Dandliker, R.D. Conner, W.L. Johnson, J. Mater. Res. 13 (1998) 2896.
[8] J.P. Holman, Heat Transfer, 6th Ed., McGraw-Hill, New York, 1986, p. 13.
[9] E.H. Lee, T.G. Rogers, T.C. Woo, J. Am. Ceram. Soc. 48 (1965) 480.
[10] T.A. Waniuk, R. Busch, A. Masuhr, W.L. Johnson, Acta Mater. 46 (1998) 5229.
[11] A. Masuhr, T.A. Waniuk, R. Busch, W.L. Johnson, Phys. Rev. Lett. 82 (1999) 2290.
[12] R. Busch, A. Masuhr, W.L. Johnson, Mater. Sci. Eng. A 304–306 (2001) 97.
[13] J.D. Ferry, Viscoelastic Properties of Polymers, 3rd Ed., Wiley, 1980, p.70.
[14] C.R. Kurkjian, Phys. Chem. Glasses 4 (1963) 128.
[15] T. Rouxel et al., Intermetallics, in press.
[16] J. Lu, PhD thesis, California Institute of Technology, 2002.
[17] K. Ohsaka, S.K. Chung, W.K. Rhim, A. Peker, D. Scruggs, W.L. Johnson, Appl. Phys. Lett. 70 (1997) 726.
[18] Metals Handbook (desk ed.), American Society for Metals, Metals Park, OH, 1985.
[19] M.B. Prime, Appl. Mech. Rev. 52 (1999) 75.
[20] W. Cheng, I. Finnie, J. Eng. Mater. Tech. 107 (1985) 181.
[21] G.S. Schajer, J. Eng. Mater. Tech. 103 (1981) 157.
[22] W. Cheng, I. Finnie, J. Eng. Mater. Tech. 115 (1993) 220.
[23] M.B. Prime, I. Finnie, J. Eng. Mater. Tech. 118 (1996) 410.

[24] M.R. Hill, W.Y. Lin, J. Eng. Mater. Tech. 124 (2) (1992) 185.
[25] W. Cheng et al., J. Eng. Mater. Tech. 116 (1994) 1.
[26] D. Suh, R.H. Dauskardt, J. Mater. Res. 17 (6) (2002) 1254.
[27] M.B. Prime, M.R. Hill, Scripta Mater. 46 (2002) 77.
[28] C.H.V. Hastenberg, P.C. Wildervanck, A.J.H. Leenen, G.G.J. Schennink, Polym. Eng. Sci. 32 (1992) 506.
[29] W.F. Zoetelief, L.F. Douven, J. Ingen Housz, Polym. Eng. Sci. 36 (1996) 1886.
[30] S.R. Yazdi, D. Retraint, J. Lu, J. Testing Eval. 28 (2000) 282.
[31] D.J. Wulpi, Understanding How Components Fail, American Society for Metals, Metals Park, OH, 1999.
[32] P. Lequeu, P. Lassince, T. Warner, G.M. Raynaud, Aircraft Eng. Aerospace Tech. 73 (2001) 147.
[33] D.A. Tanner, J.S. Robinson, R.L. Cudd, Mater. Sci. Forum 347–349 (2001) 235.